



Universiteit  
Leiden  
The Netherlands

## Magnetic imaging of spin waves and magnetic phase transitions with nitrogen-vacancy centers in diamond

Bertelli, I.

### Citation

Bertelli, I. (2021, November 24). *Magnetic imaging of spin waves and magnetic phase transitions with nitrogen-vacancy centers in diamond*. *Casimir PhD Series*. Retrieved from <https://hdl.handle.net/1887/3245183>

Version: Publisher's Version

License: [Licence agreement concerning inclusion of doctoral thesis in the Institutional Repository of the University of Leiden](#)

Downloaded from: <https://hdl.handle.net/1887/3245183>

**Note:** To cite this publication please use the final published version (if applicable).

# 3

## SPIN-WAVE THEORY

*Spin waves are collective excitations of spins in magnetic materials. In this chapter we derive expressions that are useful and recurrent in Chapters 4-6. We start by calculating the dipolar field of a planar magnetization (Section 3.1), which we need in the following sections. Starting from the Landau-Lifshits-Gilbert (LLG) equation, in Section 3.2 we derive the spin-wave susceptibility, and from that the spin-wave dispersion. We then examine which spin-wave modes are efficiently excited inductively (Section 3.3), calculate the stray fields that spin waves generate (Section 3.4) and finally show how these fields can be detected using NV magnetometry (Section 3.5) via measuring Rabi oscillations and  $T_1$  relaxometry. Importantly, from the last three sections stem equations regarding the coupling of the stray field of a microstrip with the spin waves, and of the spin-wave stray field with NV centers.*

### 3.1. STRAY FIELD OF A PLANAR MAGNETIZATION

In this section we calculate the dipolar stray field generated by a planar magnetization. This result is needed in Sections 3.2 and 3.4, where we derive the spin-wave dispersion and the stray field of a spin wave, respectively.

The magnetic field of a single magnetic dipole  $\mathbf{m}$ , located at the origin, is given by

$$\mathbf{B}(\mathbf{r}) = \mu_0 \mathbf{\Gamma}(\mathbf{r}) \mathbf{m}, \quad (3.1)$$

where  $\mathbf{\Gamma}(\mathbf{r})$  is the dipolar tensor, given by

$$\mathbf{\Gamma}(\mathbf{r}) = \frac{1}{4\pi|\mathbf{r}|^5} \begin{pmatrix} 2x^2 - y^2 - z^2 & 3xy & 3xz \\ 3xy & 2y^2 - x^2 - z^2 & 3yz \\ 3xz & 3yz & 2z^2 - x^2 - y^2 \end{pmatrix}. \quad (3.2)$$

For a magnetization  $\mathbf{M}(\mathbf{r})$ , the stray field is given by

$$\mathbf{B}(\mathbf{r}) = \mu_0 \int d\mathbf{r}' \mathbf{\Gamma}(\mathbf{r} - \mathbf{r}') \mathbf{M}(\mathbf{r}'), \quad (3.3)$$

where the components of the dipolar tensor  $\mathbf{\Gamma}(\mathbf{r} - \mathbf{r}')$  are derivatives of the Coulomb's kernel

$$\Gamma_{\alpha\beta}(\mathbf{r} - \mathbf{r}') = \frac{\partial}{\partial\alpha} \frac{\partial}{\partial\beta'} \frac{1}{4\pi|\mathbf{r} - \mathbf{r}'|} \quad \text{with } \alpha, \beta = x, y, z. \quad (3.4)$$

Later on, we analyze spin waves (in thin films) that are characterized by their wavevector. Thus, it is convenient here to remove the convolution in Eq. 3.3 by taking the 2D Fourier transform in the film plane ( $yz$ )<sup>1</sup>

$$\mathbf{B}(\mathbf{k}, x) = \mu_0 \int dx' \mathbf{\Gamma}(\mathbf{k}, x - x') \mathbf{M}(\mathbf{k}, x'), \quad (3.5)$$

where  $\mathbf{k} = k_y \hat{\mathbf{y}} + k_z \hat{\mathbf{z}}$  is in the film plane. Using [1, 2]

$$\nabla^2 \frac{1}{4\pi|\mathbf{r} - \mathbf{r}'|} = \delta(\mathbf{r} - \mathbf{r}') \quad (3.6)$$

and the identity [1–3]

$$\frac{1}{|\mathbf{r} - \mathbf{r}'|} = 2\pi \int \frac{d\mathbf{k}}{k} e^{-k|x-x'|} e^{i\mathbf{k}(\boldsymbol{\rho} - \boldsymbol{\rho}')} \quad (3.7)$$

where  $\mathbf{k}$  and  $\boldsymbol{\rho} = y\hat{\mathbf{y}} + z\hat{\mathbf{z}}$  are in the infinite  $yz$  plane, we obtain the Fourier transform of Eq. 3.4

$$\Gamma_{\alpha\beta}(\mathbf{k}, x - x') = \frac{1}{2} \begin{cases} e^{-k|x-x'|} k - 2\delta(x-x') & \text{for } \alpha = \beta = x, \\ -e^{-k|x-x'|} \frac{k_\alpha k_\beta}{k} & \text{for } \alpha, \beta = y, z, \\ -e^{-k|x-x'|} \text{sign}(x-x') i k_\alpha & \text{for } \alpha = y, z \text{ and } \beta = x. \end{cases} \quad (3.8)$$

<sup>1</sup>We are considering a thin film with infinite lateral dimensions.

Because we consider thin films, we assume that the magnetization  $\mathbf{M} = \mathbf{m}M_s$  does not vary across the film thickness<sup>2</sup>:  $\mathbf{m}(\mathbf{k}, \mathbf{x}') = \mathbf{m}(\mathbf{k})$ . We can now integrate Eq. 3.5 over the film thickness  $t$ , where the only  $x'$ -dependent components are the  $\Gamma_{\alpha\beta}$ , so that the dipolar field at  $x$  is

$$\mathbf{B}(\mathbf{k}, \mathbf{x}) = \mu_0 M_s \int_{-t}^0 dx' \Gamma(\mathbf{k}, x - x') \mathbf{m}(\mathbf{k}) = \mu_0 M_s \overline{\Gamma}(\mathbf{k}, x) \mathbf{m}(\mathbf{k}), \quad (3.9)$$

where  $\overline{(\dots)}$  indicates spatial averaging over the film thickness. Carrying out the integration for  $\mathbf{r} > \mathbf{r}'$  (i.e. above the film)<sup>3</sup> results in

$$\overline{\Gamma}(\mathbf{k}, x) = \int_{-t}^0 dx' \Gamma(\mathbf{k}, x - x') = \frac{1}{2} e^{-kx} (1 - e^{-kt}) \begin{pmatrix} -1 & i \sin \phi & i \cos \phi \\ i \sin \phi & \sin^2 \phi & \sin \phi \cos \phi \\ i \cos \phi & \sin \phi \cos \phi & \cos^2 \phi \end{pmatrix}, \quad (3.10)$$

where we expressed  $\mathbf{k}$  in terms of its polar coordinates  $k$  and  $\phi$  ( $\phi = 0$  corresponds to the  $z$  axis).

Below the magnetic film,  $\text{sign}(x - x')$  in Eq. 3.8 changes sign, so that  $\Gamma_{xy}, \Gamma_{yx}, \Gamma_{xz}, \Gamma_{zx}$  also change sign. It will become clear in Section 3.4 that this result is important to understand the chirality of NV-based detection of spin waves with  $\phi = \pm\pi/2$ .

## 3.2. SPIN-WAVE DISPERSION

The relation between the frequency of an excitation and its wavelength is known as dispersion. The gradient of the dispersion, called group velocity, denotes the direction in which energy is transported in the system. In this section we derive the transverse dynamic susceptibility of a thin magnetic film from the Landau-Lifshitz-Gilbert (LLG) equation. From the susceptibility, we find expressions for the spin-wave dispersion and damping. The LLG equation phenomenologically describes the damped motion of the magnetization in an effective magnetic field, composed of several contributions, such as the Zeeman, exchange, and dipolar interactions. In Section 3.3 we use the spin-wave susceptibility to calculate the magnetization excited inductively by a microwave stripline.

### 3.2.1. MAGNETIZATION DYNAMICS: LANDAU-LIFSHITZ-GILBERT EQUATIONS

We consider an external static magnetic field  $\mathbf{B}_0$  applied along  $z$  ( $\mathbf{B}_0 = B_0 \hat{\mathbf{z}}$ ) (Fig. 3.1), which forces the static magnetization parallel to  $z$ <sup>4,5</sup>. The magnetization evolves in time

<sup>2</sup>This assumption is valid in the limit  $kt \ll 1$ , where  $t$  is the film thickness, which is the case for the magnetization profiles in this thesis.

<sup>3</sup>For  $x > x'$ , we use  $\int_{-t}^0 dx' e^{-k|x-x'|} = \int_{-t}^0 dx' e^{-kx} e^{kx'} = e^{-kx} \frac{1 - e^{-kt}}{k}$ .

<sup>4</sup>We disregard the crystalline anisotropy, because it is small for the magnets considered in this thesis (Ni, YIG) [4].

<sup>5</sup>In the experiments of Chapters 4-5, the static field is applied along the axis of one NV center family, which forms a  $\sim 35^\circ$  angle with the  $z$  axis. However, the fields we apply in spin-wave experiments are always smaller than  $\sim 30$  mT, such that the out-of-plane component is smaller than  $\sim 17.3$  mT. Since the saturation magnetization of YIG is 178 mT at room temperature, the static magnetization tilts out-of-plane by less than  $\text{atan}(17.3/178) \sim 5.6^\circ$ . In Chapter 6, the system considered is nickel, whose saturation magnetization is  $\sim 5$  times higher, but we also apply fields up to  $\sim 60$  mT. We treat the case of a tilted magnetization in Section 3.2.3.

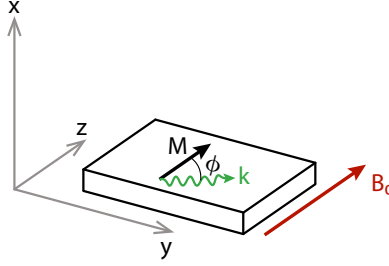


**Figure 3.1: Geometry of the system.** A thin film in the  $yz$  plane is magnetized along  $z$  by the static magnetic field  $\mathbf{B}_0$ . Spin waves propagate with wavevector  $\mathbf{k}$  at angle  $\phi$  from  $\mathbf{M}$ .

following the Landau-Lifshitz-Gilbert (LLG) equation [5]:

$$\frac{d\mathbf{m}}{dt} = -\gamma \mathbf{m} \times \mathbf{B}_{\text{eff}} - \alpha \frac{d\mathbf{m}}{dt} \times \mathbf{m}, \quad (3.11)$$

where  $\alpha$  is the Gilbert damping parameter (we study changes of  $\alpha$  due to increased damping in Chapter 5) and  $\mathbf{B}_{\text{eff}}$  is the effective magnetic field (including both static and dynamic contributions). The first term after the equal sign in Eq. 3.11 induces the precession of  $\mathbf{m}$  around  $\mathbf{B}_{\text{eff}}$  (Fig. 3.2). The second term induces a rotation of  $\mathbf{m}$  toward  $\mathbf{B}_{\text{eff}}$ , with rate given by  $\alpha$ , and is therefore a damping term. Here,  $\mathbf{B}_{\text{eff}}$  is the sum of the external fields and the effective fields due to dipolar and exchange contributions (both static and oscillating):

$$\mathbf{B}_{\text{eff}} = \mathbf{B}_0 + \mathbf{B}_{\text{AC}} + \mathbf{B}_{\text{dem}} + \mathbf{B}_{\text{ex}} \quad (3.12)$$

where  $\mathbf{B}_{\text{AC}}$  is an external oscillating field used to excite spin waves,  $\mathbf{B}_{\text{dem}}$  is the demagnetizing (i.e. dipolar) field and  $\mathbf{B}_{\text{ex}}$  the exchange field. We evaluate each contribution in the following sections.

### ZEEMAN INTERACTION

The Zeeman energy associated with the external magnetic field is

$$F_Z = -\mathbf{M} \cdot \mathbf{B}_0 = M_s \mathbf{m} \cdot \mathbf{B}_0. \quad (3.13)$$

Defining  $\omega_B = \gamma B_0$ , the Zeeman contribution to the effective field is

$$B_{0,z} = \frac{\omega_B}{\gamma}. \quad (3.14)$$

### EXCHANGE INTERACTION

The exchange interaction is short-ranged (i.e. few nanometers) and, in a magnet with negligible anisotropy constants such as YIG [4], the exchange energy density can be considered isotropic:

$$F_{\text{ex}}(\mathbf{r}) = \frac{D}{2} \sum_{i,j=x,y,z} \left( \frac{\partial m_i(\mathbf{r})}{\partial j} \right)^2. \quad (3.15)$$

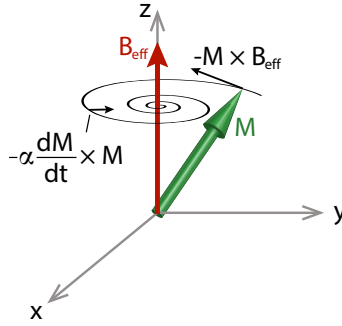


**Figure 3.2: Time evolution of the magnetization according to the LLG equation.** The magnetization  $\mathbf{M}$  precesses around the effective field  $\mathbf{B}_{\text{eff}}$  (which is static, in this sketch). The damping term forces  $\mathbf{M}$  towards  $\mathbf{B}_{\text{eff}}$ .

where  $D$  is the exchange constant. Its Fourier transform over the in-plane coordinates  $y, z$  is

$$F_{\text{ex}}(\mathbf{k}, x) = -k^2 D \left[ m_y^2(\mathbf{k}, x) + m_z^2(\mathbf{k}, x) \right] + \frac{D}{2} \sum_{i=x,y,z} \left( \frac{\partial m_i(\mathbf{k}, x)}{\partial x} \right)^2, \quad (3.16)$$

where  $\mathbf{k}$  is the spin-wavevector (in the  $yz$  plane). For a constant magnetization over the film thickness, the last term vanishes. Thus, the exchange energy contributes an effective field with Cartesian components:

$$B_{\text{ex},i} = -\frac{1}{M_s} \frac{\partial F}{\partial m_i} = -\frac{\omega_{\text{ex}}}{\gamma} k^2 m_i(\mathbf{k}, x), \quad (3.17)$$

where we defined  $\omega_{\text{ex}} = \gamma D / M_s$

### DIPOLAR INTERACTION

The dipolar interaction is long ranged and strongly anisotropic, unlike the short-ranged, isotropic exchange interaction. Therefore, the dipolar contribution leads to an anisotropic spin-wave dispersion at long wavelengths: spin waves propagating perpendicularly to the static magnetization generate a larger stray (i.e. dipolar) field than those propagating parallel to it, which costs energy.

We use the results of Section 3.1 to calculate the demagnetizing field

$$\mathbf{B}_{\text{dem}}(\mathbf{r}) = \mu_0 M_s \int \Gamma(\mathbf{r} - \mathbf{r}') \mathbf{m}(\mathbf{r}') d\mathbf{r}', \quad (3.18)$$

which can be seen as the field felt by a spin, due to the dipolar field of all the other spins in the system.

In  $k$ -space, after averaging over the film thickness, from Eq. 3.9 we obtain

$$\bar{\mathbf{B}}_{\text{dem}}(\mathbf{k}) = \mu_0 M_s \frac{1}{t} \int_{-t}^0 dx \Gamma(\mathbf{k}, x) \mathbf{m}(\mathbf{k}) = \mu_0 M_s \bar{\Gamma}(\mathbf{k}) \mathbf{m}(\mathbf{k}), \quad (3.19)$$

where  $\overline{(\dots)}$  indicates averaging over the thickness. Using Eq. 3.8 and

$$\frac{1}{t} \int_{-t}^0 \int_{-t}^0 dx' dx e^{-k|x-x'|} = \frac{2}{k} \left(1 - \frac{1 - e^{-kt}}{kt}\right) = \frac{2}{k} f(kt), \quad (3.20)$$

$$\frac{1}{t} \int_{-t}^0 \int_{-t}^0 dx' dx \text{sign}(x-x') e^{-k|x-x'|} = 0, \quad (3.21)$$

$$\frac{1}{t} \int_{-t}^0 \int_{-t}^0 dx' dx \delta(x-x') = 1, \quad (3.22)$$

we arrive at

$$\overline{\mathbf{B}}_{\text{dem}}(\mathbf{k}) = \mu_0 M_s \begin{pmatrix} f(kt) - 1 & 0 & 0 \\ 0 & \frac{-k_y^2}{k^2} f(kt) & \frac{-k_y k_z}{k^2} f(kt) \\ 0 & \frac{-k_y k_z}{k^2} f(kt) & \frac{-k_z^2}{k^2} f(kt) \end{pmatrix} \begin{pmatrix} m_x(\mathbf{k}) \\ m_y(\mathbf{k}) \\ m_z(\mathbf{k}) \end{pmatrix}, \quad (3.23)$$

which can be re-written as

$$\overline{\mathbf{B}}_{\text{dem}}(\mathbf{k}) = \mu_0 M_s \begin{pmatrix} f - 1 & 0 & 0 \\ 0 & -f \sin^2 \phi & -f \sin \phi \cos \phi \\ 0 & -f \sin \phi \cos \phi & -f \cos^2 \phi \end{pmatrix} \begin{pmatrix} m_x(\mathbf{k}) \\ m_y(\mathbf{k}) \\ m_z(\mathbf{k}) \end{pmatrix}, \quad (3.24)$$

where  $\phi$  is the in-plane angle between  $\mathbf{m}$  and  $\mathbf{k}$ . Thus, the dipolar contribution to the effective field in the LLG equations (Eq. 3.12) reads

$$\mathbf{B}_{\text{dem}}(\mathbf{k}) = \frac{\omega_{\text{dem}}}{\gamma} \overline{\Gamma}(k) \mathbf{m}(\mathbf{k}), \quad (3.25)$$

where we defined

$$\omega_{\text{dem}} = \gamma \mu_0 M_s. \quad (3.26)$$

### 3.2.2. SPIN-WAVE DISPERSION AND SUSCEPTIBILITY

Having evaluated the contributions to  $\mathbf{B}_{\text{eff}}$ , we can now calculate the spin-wave dispersion. To do so, we Fourier-transform the LLG equation (Eq. 3.11) into the frequency domain, and linearize it by assuming that  $m_z = \sqrt{1 - m_x^2 - m_y^2} \approx 1$ , yielding

$$-i\omega m_x = -\gamma(B_{\text{eff},z} m_y - B_{\text{eff},y}) + i\alpha\omega m_y, \quad (3.27)$$

$$-i\omega m_y = -\gamma(B_{\text{eff},x} - B_{\text{eff},z} m_x) - i\alpha\omega m_x. \quad (3.28)$$

Using Eq. 3.12 and  $\Gamma_{xy} = \Gamma_{yx} = 0$  (from Eq. (3.24)) we obtain

$$\gamma B_{\text{eff},x} = \omega_{\text{dem}}(f - 1) m_x - \omega_{\text{ex}} k^2 m_x + \gamma B_{\text{AC},x}, \quad (3.29)$$

$$\gamma B_{\text{eff},y} = -\omega_{\text{dem}} f \sin^2 \phi m_y - \omega_{\text{ex}} k^2 m_y + \gamma B_{\text{AC},y}, \quad (3.30)$$

$$\gamma B_{\text{eff},z} = \omega_B. \quad (3.31)$$

Defining

$$\omega_0 = \omega_B + \omega_{\text{ex}} k^2, \quad (3.32)$$

$$\omega_2 = \omega_0 + \omega_{\text{dem}}(1 - f), \quad (3.33)$$

$$\omega_3 = \omega_0 + \omega_{\text{dem}} f \sin^2 \phi, \quad (3.34)$$

we obtain Eqns. (3.27-3.28) in matrix form:

$$\begin{pmatrix} \omega_2 - i\alpha\omega & i\omega \\ -i\omega & \omega_3 - i\alpha\omega \end{pmatrix} \begin{pmatrix} m_x \\ m_y \end{pmatrix} = \gamma \begin{pmatrix} B_{AC,x} \\ B_{AC,y} \end{pmatrix}. \quad (3.35)$$

Inverting Eq. (3.35) gives the susceptibility tensor

$$\boldsymbol{\chi} = \frac{\gamma}{(\omega_2 - i\alpha\omega)(\omega_3 - i\alpha\omega) - \omega^2} \begin{pmatrix} \omega_3 - i\alpha\omega & -i\omega \\ i\omega & \omega_2 - i\alpha\omega \end{pmatrix}. \quad (3.36)$$

The matrix elements of the susceptibility tensor describe the response of the magnetization to a transverse magnetic drive field. The prefactor, with a Lorentzian-like form, peaks at a ( $k$ - and  $\phi$ -dependent) resonance frequency, and has a width that is governed by  $\alpha$ . We can find the spin-wave dispersion by solving

$$\Lambda = \omega^2 - (\omega_2 - i\alpha\omega)(\omega_3 - i\alpha\omega) = 0, \quad (3.37)$$

with solutions

$$\omega = -i\alpha \frac{\omega_2 + \omega_3}{2(1 + \alpha^2)} \pm \sqrt{\frac{4\omega_2\omega_3 - \alpha^2(\omega_2 + \omega_3)^2}{4(1 + \alpha^2)}}. \quad (3.38)$$

The real (imaginary) part of this equation gives the dispersion  $\omega_{sw}$  (linewidth  $\Delta\omega_{sw}$ )

$$\omega_{sw} \approx \sqrt{\omega_2\omega_3}, \quad (3.39)$$

$$\Delta\omega_{sw} \approx \alpha \frac{\omega_2 + \omega_3}{2}, \quad (3.40)$$

where we neglected the  $\alpha^2$  terms, since usually  $\alpha < 0.01$ . The ellipticity of the magnetization precession is given by

$$\eta = \left| \frac{\chi_{xx}}{\chi_{yx}} \right| \approx \sqrt{\frac{\omega_3}{\omega_2}}. \quad (3.41)$$

Interestingly, the dispersion of spin waves is strongly anisotropic due to the  $\phi$ -dependence of  $\omega_3$  (Fig. 3.3). We can consider three important cases:

- The mode with  $k = 0$  is spatially uniform, and known as ferromagnetic resonance (FMR). Its frequency follows from Eq. 3.39, and is given by<sup>6</sup>

$$\omega_{sw} = \sqrt{\omega_B(\omega_B + \omega_{\text{dem}})} = \gamma \sqrt{B_0(B_0 + \mu_0 M_s)}, \quad (3.42)$$

which is known as Kittel's law [6].

A typical way of studying this mode is with microwave absorption measurements, such as cavity- or broadband-FMR, which often aim at characterizing the width of the absorption dip to extract the saturation magnetization and (changes in) the Gilbert damping parameter (see Chapter 4 for an example of such measurements).

<sup>6</sup>For  $k = 0$ ,  $f \rightarrow 0$ , so that  $\omega_2 \rightarrow \omega_B + \omega_{\text{dem}}$  and  $\omega_3 \rightarrow \omega_B$ .

- Spin-waves propagating parallel to the magnetization ( $\phi = 0; \pi$ ) are known as backward-volume spin waves (BVSW), because of the negative group velocity at small  $\mathbf{k}$ . Their dispersion reads

$$\omega_{sw} = \sqrt{\omega_0[\omega_0 + \omega_{\text{dem}}(1 - f)]}, \quad (3.43)$$

and is plotted in Fig. 3.3b (red line).

- Spin waves propagating perpendicular to the magnetization ( $\phi = \pm\pi/2$ ) are known as Damon-Eshbach spin waves (DESW) [7, 8], surface spin waves, and often described with the adjective "chiral" (blue line in Fig. 3.3b). The reasons for these names are historical: the article in Ref. [7], by Eshbach and Damon, is the first to identify and study these modes that are confined to the surface in YIG crystals of macroscopic dimensions. However, the vertical confinement of these modes is on the order of the spin-wavelength (they decay exponentially with depth), so that in films thinner than  $\sim 1 \mu\text{m}$ , this confinement is effectively negligible for micron-sized spin waves. The "chiral" aspect will become clear in this chapter (Sections 3.4-3.5). Their dispersion reads

$$\omega_{sw} = \sqrt{[\omega_0 + f\omega_{\text{dem}}][\omega_0 + (1 - f)\omega_{\text{dem}}]}. \quad (3.44)$$

In the rest of this thesis, we use "BV" and "DE" to indicate the propagation direction of the spin waves with respect to the static magnetization.

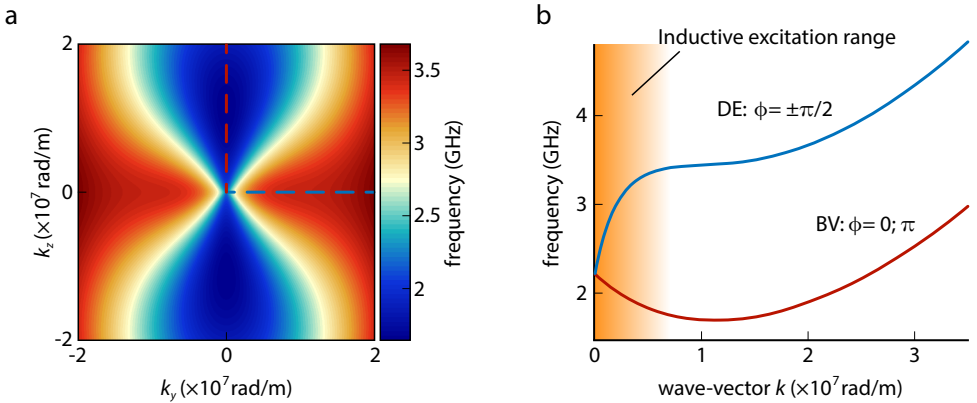


**Figure 3.3: Spin-wave dispersion.** (a) 2D spin-wave dispersion for  $B_0 = 30 \text{ mT}$ . The frequency of a spin wave strongly depends on its propagation angle ( $\phi$ ) with respect to the static magnetization ( $\mathbf{M}$ ). For backward-volume spin waves (along the dashed red line), the frequency decreases with increasing wavevector (the dispersion slope corresponds to the group velocity, from which the name "backward"). For Damon-Eshbach spin waves (dashed blue line), the group velocity is always positive. (b) Linecuts of (a), corresponding to the DE (blue line) and BV (red line) spin waves. The shaded orange area indicates which wave-vector values are easily excited inductively.

### INTRINSIC HANDEDNESS OF THE MAGNETIZATION PRECESSION

A single, isolated magnetic moment precesses around the static field always with a particular handedness, performing a circular motion with direction governed by the first cross-product in the LLG equation (Eq. 3.11). In a magnet, however, a spin also feels the field generated by its neighbours (demagnetizing field). As a result, the precessional motion becomes elliptical, as described by Eq. 4.15. However, this motion retains the same preferential handedness. It is important to keep this in mind before deriving the spin-wave excitation efficiency by a microstrip (Section 3.3). In that section we shall find out that such phenomenon has a momentum-locking character that, together with this preferential handedness of the magnetization precession, results in very spatially-asymmetric spin-wave excitation.

We can see this preferred precession handedness of the magnetization by disregarding the terms with  $\alpha$  and the dipolar terms in  $\omega_2$  and  $\omega_3$ <sup>7</sup>, so that both are equal to  $\omega_0$ , and the dispersion  $\omega \sim \omega_0$ . From Eq. 3.36 we obtain

$$\frac{m_x}{m_y} = \frac{B_x \omega_0 - i B_y \omega_0}{i B_x \omega_0 + B_y \omega_0}. \quad (3.45)$$

Clearly,  $m_y = i m_x$ : the precession is right-circularly polarized. Considering the dipolar terms we just disregarded, the polarization becomes right-handed elliptical (i.e. the out-of-plane component  $m_x$  is smaller than  $m_y$ ), which can be seen as linear superposition of right- and left-circularly polarized fields, of which the right- component is larger. We see in Section 3.3 why this is important.

### 3.2.3. STATIC FIELD WITH AN OUT-OF-PLANE COMPONENT

So far we considered  $\mathbf{B}_0$  and  $\mathbf{M}$  along  $z$ . We now generalize these results to the case of a magnetic field applied with out-of-plane angle  $\theta_B$  (from the  $z$  axis), which lifts the magnetization out of plane by  $\theta$ . In this case, it is convenient to consider the system in the magnet frame, i.e. with  $z'$  rotated out-of-plane from  $z$  around  $y$  by  $\theta$  (Fig. 3.4).

The changes to the results of the previous section are to the Zeeman and the dipolar contributions. The former becomes [3]

$$B_0, z = \frac{\omega_B}{\gamma} \rightarrow \frac{\omega_B}{\gamma} \cos(\theta_B - \theta). \quad (3.46)$$

The demagnetizing field can be obtained applying a rotation matrix

$$\mathbf{R}(\theta) = \begin{pmatrix} \cos \theta & 0 & -\sin \theta \\ 0 & 1 & 0 \\ \sin \theta & 0 & \cos \theta \end{pmatrix} \quad (3.47)$$

such that  $\mathbf{m}' = \mathbf{R}(\theta)\mathbf{m}$  and  $\mathbf{m} = \mathbf{R}^T(\theta)\mathbf{m}'$ .

<sup>7</sup>At very large  $k$ , this is a good approximation.

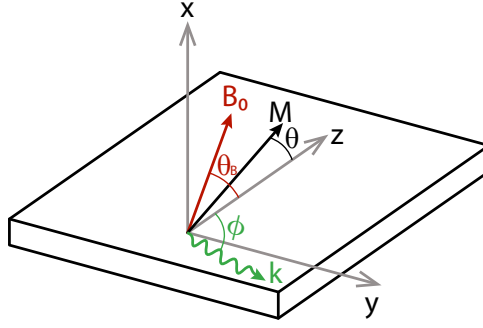


**Figure 3.4: System geometry for a magnetic field along the NV axis.** A magnetic field applied at an out-of-plane angle  $\theta_B = \theta_{NV}$  tilts the magnetization out of plane by a smaller angle  $\theta$ .

The rotated form of the dipolar tensor  $\mathbf{\Gamma}' = \mathbf{R}\mathbf{\Gamma}\mathbf{R}^T$  reads

$$\begin{pmatrix} (f-1)\cos^2\theta - f\sin^2\theta\cos^2\phi & f\sin\theta\sin\phi\cos\phi & \sin\theta\cos\theta(f-1+f\cos^2\phi) \\ f\sin\theta\sin\phi\cos\phi & -f\sin^2\phi & -f\cos\theta\sin\phi\cos\phi \\ \sin\theta\cos\theta(f-1+f\cos^2\phi) & -f\cos\theta\sin\phi\cos\phi & (f-1)\sin^2\theta - f\cos^2\theta\cos^2\phi \end{pmatrix}. \quad (3.48)$$

This modifies Eqns. 3.29 into

$$\gamma B'_{\text{eff},x} = \omega_{\text{dem}} \left\{ [(f-1)\cos^2\theta - f\sin^2\theta\cos^2\phi] m'_x + f\sin\theta\sin\phi\cos\phi m'_y \right\} - \omega_{\text{ex}} k^2 m'_x + \gamma B_{AC,x'}, \quad (3.49)$$

$$\gamma B'_{\text{eff},y} = \omega_{\text{dem}} \left[ f\sin\theta\sin\phi\cos\phi m'_x - f\sin^2\phi m'_y \right] - \omega_{\text{ex}} k^2 m'_y + \gamma B_{AC,y'}, \quad (3.50)$$

$$\gamma B'_{\text{eff},z} = \omega_B \cos(\theta_B - \theta) - \omega_{\text{dem}} \sin^2\theta, \quad (3.51)$$

where the last term in Eq. 3.51 is  $\Gamma_{zz}(k=0)$ , since  $m'_z$  is spatially homogeneous. The LLG equations in matrix form then read

$$\begin{pmatrix} \omega_2 - i\alpha\omega & -\omega_1 + i\omega \\ -\omega_1 - i\omega & \omega_3 - i\alpha\omega \end{pmatrix} \begin{pmatrix} m'_x \\ m'_y \end{pmatrix} = \gamma \begin{pmatrix} B_{AC,x'} \\ B_{AC,y'} \end{pmatrix}, \quad (3.52)$$

with

$$\omega_0 = \omega_B \cos(\theta_B - \theta) + \omega_{\text{ex}} k^2 - \omega_{\text{dem}} \sin^2\theta, \quad (3.53)$$

$$\omega_1 = \omega_{\text{dem}} f \sin\theta \sin\phi \cos\phi, \quad (3.54)$$

$$\omega_2 = \omega_0 + \omega_{\text{dem}} [(1-f)\cos^2\theta + f\sin^2\theta\cos^2\phi], \quad (3.55)$$

$$\omega_3 = \omega_0 + \omega_{\text{dem}} f \sin^2\phi. \quad (3.56)$$

The susceptibility then reads

$$\chi = \frac{\gamma}{(\omega_2 - i\alpha\omega)(\omega_3 - i\alpha\omega) - \omega_1^2 - \omega^2} \begin{pmatrix} \omega_3 - i\alpha\omega & -\omega_1 + i\omega \\ -\omega_1 - i\omega & \omega_2 - i\alpha\omega \end{pmatrix} \quad (3.57)$$

and, disregarding the terms with  $\alpha$ , the dispersion is given by

$$\omega_{sw} = \sqrt{\omega_2\omega_3 - \omega_1^2}, \quad (3.58)$$

while the linewidth is unchanged.

### 3.3. SPIN-WAVE EXCITATION

Spin waves can be excited using several methods, such as thermally [9–11], by light pulses [12], mechanically via magnetoelastic coupling [13, 14], by spin pumping via the spin-Hall effect [15, 16] or FMR-driving [17], via spin-orbit [18] and spin-transfer torques [19, 20], and inductively [21–25]. In this thesis we always use the last method because 1) we already have the necessary circuit elements, which we use to drive NV centers and 2) it allows to drive spin-waves that are coherent and monochromatic<sup>8</sup>.

In the next section we show how certain magnetization patterns and dynamics are excited using the monochromatic microwave field from a microwave stripline. We shall find out that only spin waves with specific values of  $\mathbf{k}$  can be excited, and that the excitation efficiency depends on the direction and handedness/chirality of the modes.

#### 3.3.1. INDUCTIVE EXCITATION OF SPIN-WAVES

We saw previously that the precession of the magnetization around its equilibrium position possesses a certain intrinsic handedness. In this section we shall find out that a microstrip stray field is also circularly-polarized with handedness that depends on the wave-vector  $\mathbf{k}$ . The combined result of these two phenomena is a strong spatial asymmetry in the spin-wave excitation.

In this thesis we use current-carrying circuit elements to generate an oscillating magnetic field  $\mathbf{B}$  that excites oscillations of the magnetization  $\mathbf{M}$ <sup>9</sup>

$$\mathbf{M}(\mathbf{r}) = \frac{1}{\mu_0} \int d\mathbf{r}' \chi(\mathbf{r}, \mathbf{r}') \mathbf{B}(\mathbf{r}'). \quad (3.59)$$

We can remove the convolution in the  $yz$  plane with a 2D Fourier transform that yields, in the mixed position and momentum space

$$\mathbf{M}(x, \mathbf{k}, \omega) = \frac{1}{\mu_0 t} \int_{-t}^0 dx' \chi(x, x', \mathbf{k}, \omega) \mathbf{B}(x', \mathbf{k}, \omega), \quad (3.60)$$

where  $\chi$  is the magnetic susceptibility tensor from Eq. 3.36.

We start from the stray field generated by a current distribution  $\mathbf{J}$ , using Ampere's law [1]

$$\mathbf{B}(\mathbf{r}) = \frac{\mu_0}{4\pi} \int d\mathbf{r}' \mathbf{J}(\mathbf{r}') \times \frac{\mathbf{r} - \mathbf{r}'}{|\mathbf{r} - \mathbf{r}'|^3} = \frac{\mu_0}{4\pi} \nabla \times \int d\mathbf{r}' \frac{\mathbf{J}(\mathbf{r}')}{|\mathbf{r} - \mathbf{r}'|}. \quad (3.61)$$

<sup>8</sup>The range of  $\mathbf{k}$  excited depends on the spin-wave linewidth, since the signal generated by the microwave source is extremely narrow (i.e.  $\sim$  kHz width for a GHz signal).

<sup>9</sup>Strictly speaking, in Eq. 3.59-3.60  $\mathbf{B}$  should be substituted by  $\mu_0 \mathbf{H}$ . However, we use  $\mathbf{B}$  for simplicity.

where  $\mu_0$  is the magnetic permeability of vacuum. Because  $\nabla \cdot \mathbf{B} = 0$ ,  $\mathbf{B}$  can be written as the curl of a vector potential  $\mathbf{A}$ :

$$\mathbf{B}(\mathbf{r}) = \nabla \times \mathbf{A}(\mathbf{r}). \quad (3.62)$$

From Eq. 3.61 we get

$$\mathbf{A}(\mathbf{r}, \omega) = \frac{\mu_0}{4\pi} \int d\mathbf{r}' \frac{\mathbf{J}(\mathbf{r}', \omega) e^{ik|\mathbf{r}-\mathbf{r}'|}}{|\mathbf{r}-\mathbf{r}'|}, \quad (3.63)$$

where  $k = \omega/c = \sqrt{k_x^2 + k_y^2 + k_z^2}$  with  $c$  the speed of light. We consider a microstrip of width  $w$ , length  $L$  and thickness  $h$  with current flowing parallel to  $z$ , thus  $\mathbf{A} = A\hat{z}$ , so that  $B_z = 0$ .

Eq. 3.62 then becomes

$$(B_x, B_y) = (\partial A_z / \partial y, \partial A_z / \partial x). \quad (3.64)$$

Substituting the Weyl identity<sup>10</sup> and carrying out the differentiation and integration, we obtain the Fourier components of the stray field in reciprocal space [28]:

$$B_{x(y)}(x, k_y, k_z) = 2i\mu_0 J(\omega) \frac{e^{-ik_x x}}{k_x} \frac{e^{ik_x h} - 1}{k_{x(y)}} \sin\left(k_y \frac{w}{2}\right) \sin\left(k_z \frac{L}{2}\right) \frac{e^{-ik_z z}}{k_z}, \quad (3.65)$$

where  $z = 0$  is located at the center of the microstrip. At the few-GHz frequency we consider in the experiments,  $k = \omega/c \ll 100$  rad/m, while typical spin-wavevectors for our experiments are  $10^5 - 10^7$  rad/m, so that  $k_x = \sqrt{k^2 - k_y^2 - k_z^2} \rightarrow i\sqrt{k_y^2 + k_z^2} = i\kappa$ . Thus,

$$B_x(x, k_y, k_z) = -2i\mu_0 J(\omega) e^{\kappa x} \frac{e^{-\kappa h} - 1}{\kappa^2} \sin\left(k_y \frac{w}{2}\right) \sin\left(k_z \frac{L}{2}\right) \frac{e^{-ik_z z}}{k_z}, \quad (3.66)$$

$$B_y(x, k_y, k_z) = 2\mu_0 J(\omega) e^{\kappa x} \frac{e^{-\kappa h} - 1}{\kappa k_y} \sin\left(k_y \frac{w}{2}\right) \sin\left(k_z \frac{L}{2}\right) \frac{e^{-ik_z z}}{k_z}. \quad (3.67)$$

These expressions for the field of a microstrip are useful for further calculations and offer the following insights:

- Only certain values of the spin-wavevector can be excited with a microstrip. Specifically, when an integer number of wavelengths fits under the microstrip width ( $k = n \cdot 2\pi/w$ ), the excitation efficiency vanishes. A wire that is very long in a certain direction ( $z$  in all experiments) can efficiently excite only large wavenumbers (i.e. with wavelength  $\sim$ larger than the length) in the same direction. Similarly, it is less efficient to excite spin waves with wavelength below  $1 \mu\text{m}$  with strips that are wider than a micrometer (Fig. 3.5). This difficulty in exciting nanometer-sized spin waves is a drawback of inductive spin-wave excitation.
- The polarization of the microstrip field depends on the value of  $\mathbf{k}$ . Because  $B_x = -iB_y k_y / \kappa$  (from Eqs. 3.66-3.67), we can identify two interesting situations:

<sup>10</sup>The Weyl identity is [26, 27]  $\frac{e^{ik\sqrt{(x-x')^2+(y-y')^2+(z-z')^2}}}{\sqrt{(x-x')^2+(y-y')^2+(z-z')^2}} = \frac{i}{2\pi} \int dk_y dk_z \frac{e^{ik_x|x-x'|+ik_y(y-y')+ik_z(z-z')}}{k_x}$ .

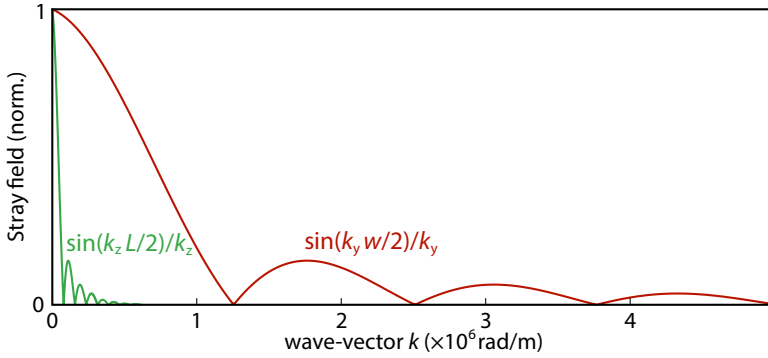


**Figure 3.5: Effect of the microstrip shape on the stray field.** A microstrip of length  $L = 100 \mu\text{m}$  (along  $z$ ) and width  $w = 5 \mu\text{m}$  (along  $y$ ) can excite spin waves with large  $k_y$  (red line) and small  $k_z$  (green line).

- When  $|k_z| \gg |k_y|$  (BV waves),  $|B_x| \ll |B_y|$ , so that the field is linearly polarized along  $\hat{y}$ .
- When  $|k_y| \gg |k_z|$  (DE waves),  $B_x \rightarrow -i \text{sign}(k_y) B_y$  represents a circularly polarized field<sup>11</sup> with opposite handedness for  $\pm k_y$  (Fig. 3.6a): Even though the stripline field is linearly polarized at each location, its right-circular (left-circular) component couples only to modes propagating with wavevector  $+k_y$  ( $-k_y$ ).
- Spin waves are preferentially excited in certain directions, i.e. their amplitude depends on  $\mathbf{k}$ . For  $|k_y| \gg |k_z|$  we have
  - For  $+k_y$ , from  $B_y = iB_x$  and Eq. 3.36 follows that  $m_y = i m_x / \eta$ , where  $\eta = |m_x| / |m_y|$  has been defined in Section 3.2.2, and<sup>12</sup>

$$m_y \approx B_y \omega_2 (1 + \eta). \quad (3.68)$$

- For  $-k_y$ , from  $B_y = -iB_x$  follows that  $m_y = -i m_x / \eta$ , with

$$m_y \approx B_y \omega_2 (1 - \eta). \quad (3.69)$$

Thus, we see from Eq. 3.68-3.69 that the spin-wave amplitude is strongly asymmetric: spin waves with circular precession (i.e.  $\eta = 1$ ) are exclusively excited with  $+k_y$ ,

<sup>11</sup>Using Jones matrices [29], we can write an oscillating field as  $B = \begin{pmatrix} B_x \\ B_y e^{i\varphi} \end{pmatrix}$ . A field for which  $B_y = \pm i B_x$

can be written as  $B = B_x \begin{pmatrix} 1 \\ \pm i \end{pmatrix} = \begin{pmatrix} 1 \\ e^{\pm i\pi/2} \end{pmatrix}$ , such that  $B_y$  trails (leads)  $B_x$  by  $\pi/2$ : the field is right-circularly (left-circularly) polarized.

<sup>12</sup>Here we are again disregarding the terms in  $\alpha$  in Eq. 3.36.

thus propagating along  $+y$ . As the precession becomes more elliptical, the left-propagating spin waves are also excited, but with very low efficiency. This strongly asymmetric excitation of DE waves by a microstrip can be seen in Chapters 4-5.

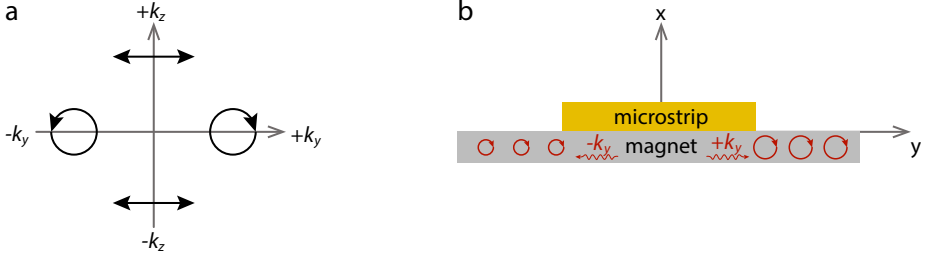


**Figure 3.6: Chiral inductive excitation of DESW by a microstrip field.** (a) For  $\mathbf{k} = \pm k_z$ , the microstrip field (black arrows) is linearly polarized along  $y$ . For  $\mathbf{k} = +k_y(-k_y)$ , the field is right(left)-circularly polarized in the  $xy$  plane. (b) The right(left)-propagating spin waves (in red) are excited with large (small) amplitude.

From the susceptibility (Eq. 3.36) and the microstrip field (Eqs. 3.66-3.67), we can calculate the dynamic magnetization in  $k$ -space using Eq. 3.60, and Fourier-transforming back into real space yields

$$M_i(\boldsymbol{\rho}, t) = \frac{1}{4\pi^2} \int \int d\mathbf{k} e^{i\mathbf{k}\cdot\boldsymbol{\rho} - i\omega t} M_i(x, \mathbf{k}), \quad (3.70)$$

where  $\boldsymbol{\rho} = (y, z)$ .

### 3.4. STRAY FIELD OF A SPIN WAVE

We can now derive the stray field of a spin wave of in-plane wavevector  $\mathbf{k}$  and frequency  $\omega/2\pi$  from Eqs. 3.9-3.10:

$$B_{sw,x}(x, \mathbf{k}) = \frac{\mu_0 M_s}{2} e^{-kx} (1 - e^{-kt}) (-m_x(\mathbf{k}) + i \sin \phi m_y(\mathbf{k})), \quad (3.71)$$

$$B_{sw,y}(x, \mathbf{k}) = \frac{\mu_0 M_s}{2} e^{-kx} (1 - e^{-kt}) (i \sin \phi m_x(\mathbf{k}) + \sin^2 \phi m_y(\mathbf{k})), \quad (3.72)$$

$$B_{sw,z}(x, \mathbf{k}) = \frac{\mu_0 M_s}{2} e^{-kx} (1 - e^{-kt}) (i \cos \phi m_x(\mathbf{k}) + \sin \phi \cos \phi m_y(\mathbf{k})), \quad (3.73)$$

where again  $\sin \phi = k_y/k$  and  $\cos \phi = k_z/k$ , so that  $B_{sw,y} = -i(k_y/k)B_{sw,x}$  and  $B_{sw,z} = -i(k_z/k)B_{sw,x}$ .

Because we use NV centers to study spin waves via their stray fields, these results are central to this thesis. Let's examine a few interesting cases:

- For  $\phi = 0(\pi)$  (BV geometry),  $B_{sw,y} = 0$  and  $B_{sw,z} = -(+ )iB_{sw,x}$ . In the  $xy$  plane, however, this field is linearly polarized.

- In the DE geometry the situation is dramatically different. For  $\phi = +\pi/2$  the spin waves propagate with  $+k_y$ , therefore  $m_y = i m_x / \eta$  (from Section 3.3) and  $B_{sw,y} = -i B_{sw,x}$ . This field is circularly polarized in the  $xy$  plane, with handedness opposite to that of the microstrip stray field, which excited the spin-waves along  $+k_y$  in the first place (Eqs. 3.66-3.67).
- For  $\phi = -\pi/2$ ,  $B_{sw,y} = +i B_{sw,x}$ . Because these modes propagate toward  $-k_y$ , they are characterized by  $m_y = -i m_x / \eta$ . Using this relation, we see that both  $B_{sw,x}$  and  $B_{sw,y}$  vanish (remembering that the formula for the stray fields holds above the magnetic film, while below the film the terms containing  $i$  change sign, see Section 3.1).

Let's summarize the importance of these results (Fig. 3.7):

- The right-propagating DE spin waves ( $+k_y$ ) generate a stray field above the magnetic film that is left-circularly polarized. If there was an ensemble of NV centers above the film, with axes parallel to the magnetic  $z$  axis, the spin-wave field would have the correct handedness to drive the  $0 \leftrightarrow -1$  NV transition of those NVs on the right of the microstrip, and would not drive the  $0 \leftrightarrow +1$  transition. However, there is usually an angle between the two axes, so that the field drives the  $0 \leftrightarrow +1$  transition as well.
- The left-propagating spin waves are not efficiently excited and generate a left-circularly polarized stray field below the film. Above the film, the field is zero for  $\eta = 1$ , and non-zero for smaller ellipticity, but with opposite handedness, such that it can drive the  $0 \leftrightarrow +1$  NV transition.
- BV waves generate a field in the  $xz$  plane. Its projection onto the  $xy$  plane (relevant to NV driving) is a linear field (for any out-of-plane angle between the NV and the magnet), which drives both transitions with equal efficiency.

### 3.5. SPIN-WAVE DETECTION WITH NV MAGNETOMETRY

In this section we derive the effect of the stray field of coherent (Section 3.5.1) and thermal (Section 3.5.2) spin waves on the NV center spin state.

#### 3.5.1. DETECTING COHERENT SPIN WAVES: RABI FREQUENCY ENHANCEMENT

In Chapter 4 we measure the NV Rabi frequency induced by the stray field of spin waves to image them and ultimately extract the amplitude of the spin-wave oscillations. In Chapter 5 we detect a change in spin-wave damping by measuring the spatial variations of the Rabi frequency. In this section we derive the Rabi frequency induced by the spin-wave stray field.

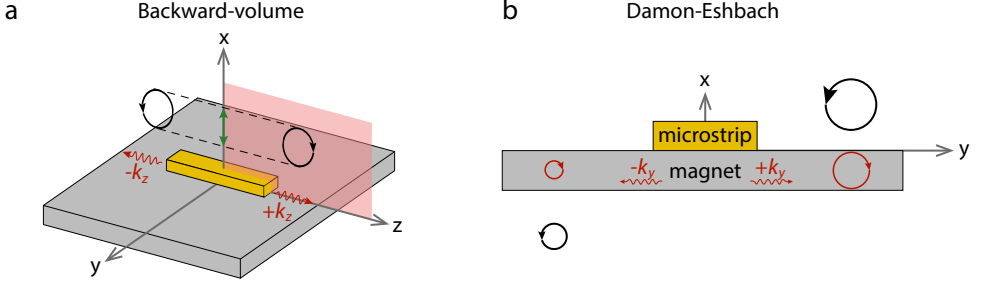


**Figure 3.7: Momentum-locked spin-wave handedness.** (a) Backward-volume spin waves (red arrows) generate fields that are circularly-polarized in the  $xz$  plane (black arrows). In the  $xy$  plane, the field is linearly polarized (green arrow). (b) Damon-Eshbach spin waves (red arrows) are excited with different amplitudes on the two sides of the stripline. The field they generate (black arrows) is circularly-polarized in the  $xy$  plane, with handedness opposite to that of the spin precession. Right-propagating spin waves generate a large left-circular field above the magnetic film. Conversely, left-propagating spin waves (less efficiently excited) generate a left-circular field below the film. If we consider spin waves with an elliptical precession (i.e.  $\eta < 1$ ), a small field component is present also below (above) the film, on the right (left) side, that has the opposite handedness of the component above (below).

We know from 2.17 that the  $\omega_{\pm}$  transition is driven by a resonant magnetic field that is circularly polarized in the plane perpendicular to the NV axis, inducing Rabi rotations with frequency  $\Omega_R^{\pm} = \gamma|B_x \mp iB_y|/\sqrt{2}$ . We can use the results of the previous section for the spin-wave field, but we need to transform them into the NV reference frame (rotated by  $\theta_{NV}$  from  $z$  toward  $x$  about  $y$ ). To do so, we use the rotation matrix of Eq. 3.47 to obtain the  $\mathbf{B}_+$  component in the NV frame:

$$|\mathbf{B}_+^{NV}| = |B_x \cos\theta_{NV} - B_z \sin\theta_{NV} + iB_y|. \quad (3.74)$$

For spin waves propagating along  $+k_y$ , we obtain

$$\Omega_R^{\pm} = |B_{sw}^0 m_y| \frac{\gamma \sqrt{\eta^2 + \sin^2 \phi}}{\sqrt{2}} \sqrt{(\cos\theta_{NV} \pm \sin\phi)^2 + \sin^2\theta_{NV} \cos^2\phi}, \quad (3.75)$$

where  $B_{sw}^0 = \mu_0 M_s e^{-kx} (1 - e^{-kt})/2$ .

We see that, for BVSWs ( $\phi = 0, \pi$ ),  $\Omega_R^{\pm} = |B_{sw}^0 m_y \eta / \sqrt{2}|$ , so that  $\omega_{\pm}$  are driven equally. Moreover, when the waves are very elliptical<sup>13</sup> (small  $\eta$ ) the spin-wave driving of the NV transitions decreases correspondingly.

For  $\phi = \pi/2$ ,  $\Omega_R^{\mp} = |B_{sw}^0 m_y| \sqrt{\eta^2 + 1} |\cos\theta_{NV} \pm 1| / \sqrt{2}$ . As previously introduced, for  $\theta_{NV} = 0$ , the spin-wave field is circularly polarized in the NV- $xy$  axis and only drives  $\omega^-$ .

<sup>13</sup>At large wavelengths, the out-of-plane component is much smaller than the in-plane one [28].

In Chapter 4 we build on this model, considering the additional stray field components of a microwave stripline and of a bonding wire, used as antenna, to extract the precession amplitude of DE spin waves from experiments. In Chapter 5 we monitor the spatial decay of the Rabi frequency to characterize the spin-wave damping induced by metallic electrodes.

### 3.5.2. MAGNETIC NOISE GENERATED BY THERMALLY-EXCITED SPIN WAVES

Even in absence of direct driving, incoherent spin waves are thermally excited because of the finite temperature. Such spin waves generate fluctuating magnetic fields that act as noise and can induce relaxation of the NV spin states. In Chapter 6, we probe these magnetic fluctuations in a nickel thin film using NV relaxometry. In this section we derive the magnetic field noise generated by these thermal spin-waves, and calculate the NV relaxation rates they induce.

The system considered is a thin magnetic film in the  $yz$  plane. A single NV center is located at distance  $d$  above the film, with axis oriented in the  $xz$  plane at an angle  $\theta_{NV}$  from  $z$ . A static field is applied along the NV axis, which lifts the magnetization of the film out of plane by an angle  $\theta$ . From Eq. 3.9, 3.10, and the rotation matrix  $\mathbf{R}(\theta)$  (Eq. 3.47) the dipolar field in the NV frame is given by

$$\mathbf{B}_{NV} = M_s \mathbf{R}(\theta_{NV}) \mathbf{\Gamma}(\mathbf{k}) \mathbf{R}^T(\theta) \mathbf{m}'(\mathbf{k}) = M_s \mathbf{\Gamma}^{\text{eff}}(\mathbf{k}) \mathbf{m}'(\mathbf{k}). \quad (3.76)$$

Substituting into Eq. 2.20, we can express the relaxation rates as an integral over  $k$ -space [3]

$$\Gamma_{\mp} = \frac{\gamma^2 M_s^2}{2} \int \frac{d\mathbf{k}}{(2\pi)^2} \sum_{i,j=\{x,y\}} \Gamma_{\pm i}^{\text{eff}}(\mathbf{k}) \Gamma_{\mp j}^{\text{eff}}(-\mathbf{k}) C_{ij}(\mathbf{k}, \omega_{\mp}), \quad (3.77)$$

where the elements of the dipolar tensor  $\Gamma_{\pm i}^{\text{eff}} = \Gamma_{xi}^{\text{eff}} \pm i \Gamma_{yi}^{\text{eff}}$  and  $C_{ij}$  is the Fourier transform of the magnetization correlator [3, 30]

$$C_{ij}(\mathbf{r} - \mathbf{r}', t - t') = \langle m'_i(\mathbf{r}, t) m'_j(\mathbf{r}', t') \rangle. \quad (3.78)$$

The magnetization correlations are governed by the dispersion and the band occupation, determined by the temperature  $T$ . Defining  $D_{\text{th}} = \alpha k_B T / (\gamma M_s t)$ , with  $k_B$  the Boltzmann constant, we can express the  $C_{ij}$  as [3]

$$C_{ij}(\mathbf{k}, \omega) = 2D_{\text{th}} \sum_{\rho=\{x,y\}} \chi_{i\rho}(\mathbf{k}, \omega) \chi_{j\rho}(-\mathbf{k}, -\omega), \quad (3.79)$$

where  $\chi_{ij}$  are the elements of the susceptibility in Eq. 3.57 (for  $\theta_B = \theta_{NV}$ ).

In the next chapter we see that these equations agree quite well with the measured relaxation rates. Unlike previous models [17, 31, 32], which only included in-plane oscillations of the magnetization (thus, the spin-wave fields were linearly polarized, coupling equally well to both NV ESR transitions), this model includes the handedness of the spin-waves and their fields, which therefore couple differently to the two NV ESR transitions. Thus, this model can be applied without arbitrary scaling constant to account for the

different rates at  $\omega_{\pm}$ . We use this in Chapter 6 to calculate the NV relaxation rate as a function of the static field (Fig. 3.8).

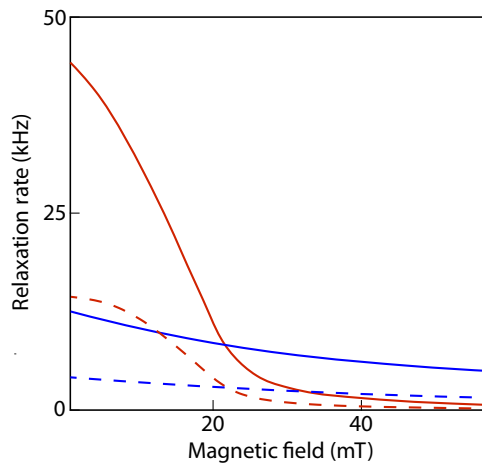


**Figure 3.8: NV relaxation rate as a function of magnetic field.** Red (blue) lines: calculated relaxation rate of the  $|0\rangle \leftrightarrow |-1\rangle$  ( $|0\rangle \leftrightarrow |+1\rangle$ ) transition, for a distance of 200 nm (solid lines) and 300 nm (dashed lines) between an NV center and a nickel film of thickness 40 nm.

## REFERENCES

- [1] J. D. Jackson, *Classical Electrodynamics* (Wiley, New York, 1998).
- [2] K. Y. Guslienko and A. N. Slavin, *Magnetostatic Greens functions for the description of spin waves in finite rectangular magnetic dots and stripes*, *Journal of Magnetism and Magnetic Materials* **323**, 2418 (2011).
- [3] A. Rustagi, I. Bertelli, T. Van Der Sar, and P. Upadhyaya, *Sensing chiral magnetic noise via quantum impurity relaxometry*, *Physical Review B* **102**, 220403 (2020).
- [4] D. D. Stancil and A. Prabhakar, *Spin waves* (Springer, New York, 2009).
- [5] T. L. Gilbert, *A phenomenological theory of damping in ferromagnetic materials*, *IEEE Transactions on Magnetics* **40**, 3443 (2004).
- [6] C. Kittel, *Introduction to Solid State Physics*, 8th ed. (Wiley, 2005).
- [7] J. R. Eshbach and R. W. Damon, *Surface magnetostatic modes and surface spin waves*, *Physical Review* **118**, 1208 (1960).
- [8] R. W. Damon and J. R. Eshbach, *Magnetostatic modes of a ferromagnet slab*, *Journal of Physics and Chemistry of Solids* **19**, 308 (1961).
- [9] K. Uchida, S. Takahashi, K. Harii, J. Ieda, W. Koshibae, K. Ando, S. Maekawa, and E. Saitoh, *Observation of the spin Seebeck effect*, *Nature* **455**, 778 (2008).
- [10] J. Xiao, G. E. Bauer, K. C. Uchida, E. Saitoh, and S. Maekawa, *Theory of magnon-driven spin Seebeck effect*, *Physical Review B* **81**, 214418 (2010).
- [11] M. Schneider, T. Brächer, D. Breitbach, V. Lauer, P. Pirro, D. A. Bozhko, H. Y. Musiienko-Shmarova, B. Heinz, Q. Wang, T. Meyer, F. Heussner, S. Keller, E. T. Papaioannou, B. Lägel, T. Löber, C. Dubs, A. N. Slavin, V. S. Tiberkevich, A. A. Serga, B. Hillebrands, and A. V. Chumak, *Bose–Einstein condensation of quasiparticles by rapid cooling*, *Nature Nanotechnology* **15**, 457 (2020).
- [12] T. Kampfrath, A. Sell, G. Klatt, A. Pashkin, S. Mährlein, T. Dekorsy, M. Wolf, M. Fiebig, A. Leitenstorfer, and R. Huber, *Coherent terahertz control of antiferromagnetic spin waves*, *Nature Photonics* **5**, 31 (2011).
- [13] M. Weiler, L. Dreher, C. Heeg, H. Huebl, R. Gross, M. S. Brandt, and S. T. Goennenwein, *Elastically driven ferromagnetic resonance in nickel thin films*, *Physical Review Letters* **106**, 117601 (2011).
- [14] X. Li, D. Labanowski, S. Salahuddin, and C. S. Lynch, *Spin wave generation by surface acoustic waves*, *Journal of Applied Physics* **122**, 43904 (2017).
- [15] L. J. Cornelissen, J. Liu, R. A. Duine, J. B. Youssef, and B. J. Van Wees, *Long-distance transport of magnon spin information in a magnetic insulator at room temperature*, *Nature Physics* **11**, 1022 (2015).

- [16] L. J. Cornelissen, J. Liu, B. J. van Wees, and R. A. Duine, *Spin-Current-Controlled Modulation of the Magnon Spin Conductance in a Three-Terminal Magnon Transistor*, *Physical Review Letters* **120**, 097702 (2018).
- [17] C. Du, T. van der Sar, T. X. Zhou, P. Upadhyaya, F. Casola, H. Zhang, M. C. Onbasli, C. A. Ross, R. L. Walsworth, Y. Tserkovnyak, and A. Yacoby, *Control and local measurement of the spin chemical potential in a magnetic insulator*, *Science* **357**, 195 (2017).
- [18] M. Collet, X. De Milly, A. Kelly, V. V. Naletov, R. Bernard, P. Bortolotti, J. B. Youssef, V. E. Demidov, S. O. Demokritov, J. L. Prieto, M. Muñoz, V. Cros, A. Anane, G. De Loubens, and O. Klein, *Generation of coherent spin-wave modes in yttrium iron garnet microdiscs by spin-orbit torque*, *Nature Communications* **7**, 10377 (2016).
- [19] S. I. Kiselev, J. C. Sankey, I. N. Krivorotov, N. C. Emley, R. J. Schoelkopf, R. A. Buhrman, and D. C. Ralph, *Microwave oscillations of a nanomagnet driven by a spin-polarized current*, *Nature* **425**, 380 (2003).
- [20] K. J. Lee, A. Deac, O. Redon, J. P. Nozières, and B. Dieny, *Excitations of incoherent spin-waves due to spin-transfer torque*, *Nature Materials* **3**, 877 (2004).
- [21] C. Kittel, *On the theory of ferromagnetic resonance absorption*, *Physical Review* **73**, 155 (1948).
- [22] L. R. Walker, *Magnetostatic modes in ferromagnetic resonance*, *Physical Review* **105**, 390 (1957).
- [23] S. O. Demokritov, V. E. Demidov, O. Dzyapko, G. A. Melkov, A. A. Serga, B. Hillebrands, and A. N. Slavin, *Bose-Einstein condensation of quasi-equilibrium magnons at room temperature under pumping*, *Nature* **443**, 430 (2006).
- [24] C. W. Sandweg, Y. Kajiwara, A. V. Chumak, A. A. Serga, V. I. Vasyuchka, M. B. Jungfleisch, E. Saitoh, and B. Hillebrands, *Spin pumping by parametrically excited exchange magnons*, *Physical Review Letters* **106**, 216601 (2011).
- [25] I. S. Maksymov and M. Kostylev, *Broadband stripline ferromagnetic resonance spectroscopy of ferromagnetic films, multilayers and nanostructures*, *Physica E: Low-Dimensional Systems and Nanostructures* **69**, 253 (2015).
- [26] L. Novotny and B. Hecht, *Principles of nano-optics*, 2nd ed. (Cambridge University Press, Cambridge, 2006).
- [27] H. Weyl, *Ausbreitung elektromagnetischer Wellen über einem ebenen Leiter*, *Annalen der Physik* **365**, 481 (1919).
- [28] I. Bertelli, J. J. Carmiggelt, T. Yu, B. G. Simon, C. C. Pothoven, G. E. Bauer, Y. M. Blanter, J. Aarts, and T. van der Sar, *Magnetic resonance imaging of spin-wave transport and interference in a magnetic insulator*, *Science advances* **6**, eabd3556 (2020).
- [29] E. Hecht, *Optics*, 4th ed. (Pearson, 2002).

- [30] B. Flebus and Y. Tserkovnyak, *Quantum-Impurity Relaxometry of Magnetization Dynamics*, *Physical Review Letters* **121**, 187204 (2018).
- [31] T. van der Sar, F. Casola, R. Walsworth, and A. Yacoby, *Nanometre-scale probing of spin waves using single-electron spins*, *Nature Communications* **6**, 1 (2015).
- [32] C. M. Purser, V. P. Bhallamudi, F. Guo, M. R. Page, Q. Guo, G. D. Fuchs, and P. C. Hammel, *Spinwave detection by nitrogen-vacancy centers in diamond as a function of probe-sample separation*, *Applied Physics Letters* **116**, 202401 (2020).

